

## RESEARCH ARTICLE

10.1002/2015JC010774

## Key Points:

- Vertical variability of particle abundance is size dependent
- Phytoplankton community structure partly determines variability in PSD
- Power law parameterizations of the PSD are sensitive to the fitting procedure

## Correspondence to:

B. Barone,  
benedetto.barone@gmail.com

## Citation:

Barone, B., R. R. Bidigare, M. J. Church, D. M. Karl, R. M. Letelier, and A. E. White (2015), Particle distributions and dynamics in the euphotic zone of the North Pacific Subtropical Gyre, *J. Geophys. Res. Oceans*, 120, 3229–3247, doi:10.1002/2015JC010774.

Received 7 FEB 2015

Accepted 1 APR 2015

Accepted article online 7 APR 2015

Published online 3 MAY 2015

## Particle distributions and dynamics in the euphotic zone of the North Pacific Subtropical Gyre

Benedetto Barone<sup>1,2</sup>, Robert R. Bidigare<sup>1,2</sup>, Matthew J. Church<sup>1,2</sup>, David M. Karl<sup>1,2</sup>, Ricardo M. Letelier<sup>1,3</sup>, and Angelique E. White<sup>1,3</sup>
<sup>1</sup>Daniel K. Inouye Center for Microbial Oceanography: Research and Education, Honolulu, Hawaii, USA, <sup>2</sup>Department of Oceanography, University of Hawaii, Honolulu, Hawaii, USA, <sup>3</sup>College of Earth, Ocean, and Atmospheric Sciences, Oregon State University, Corvallis, Oregon, USA

**Abstract** During the summer of 2012, we used laser diffractometry to investigate the temporal and vertical variability of the particle size spectrum (1.25–100  $\mu\text{m}$  in equivalent diameter) in the euphotic zone of the North Pacific Subtropical Gyre. Particles measured with this optical method accounted for  $\sim 40\%$  of the particulate carbon stocks ( $< 202 \mu\text{m}$ ) in the upper euphotic zone (25–75 m), as estimated using an empirical formula to transform particle volume to carbon concentrations. Over the entire vertical layer considered (20–180 m), the largest contribution to particle volume corresponded to particles between 3 and 10  $\mu\text{m}$  in diameter. Although the exponent of a power law parameterization suggested that larger particles had a lower relative abundance than in other regions of the global ocean, this parameter and hence conclusions about relative particle abundance are sensitive to the shape of the size distribution and to the curve fitting method. Results on the vertical distribution of particles indicate that different size fractions varied independently with depth. Particles between 1.25 and 2  $\mu\text{m}$  reached maximal abundances coincident with the depth of the chlorophyll *a* maximum (averaging  $121 \pm 10 \text{ m}$ ), where eukaryotic phytoplankton abundances increased. In contrast, particles between 2 and 20  $\mu\text{m}$  tended to accumulate just below the base of the mixed layer ( $41 \pm 14 \text{ m}$ ). Variability in particle size tracked changes in the abundance of specific photoautotrophic organisms (measured with flow cytometry and pigment concentration), suggesting that phytoplankton population dynamics are an important control of the spatiotemporal variability in particle concentration in this ecosystem.

## 1. Introduction

Suspended particulate matter in the sea includes living organisms (protists, zooplankton, bacteria, and archaea), detritus, and mineral particles. This material is often quantified by measuring total mass or specific element content (including isotopes) from particles collected with nets or concentrated onto filters. For example, our understanding of particulate matter inventories and dynamics in the North Pacific Subtropical Gyre (NPSG) has been greatly aided by vertically resolved, near-monthly measurements of total particulate carbon, nitrogen, and phosphorus concentrations (PC, PN, and PP, respectively) conducted over the past 25 years at Station ALOHA ( $22^\circ 45' \text{N}$ ,  $158^\circ \text{W}$ ) by the Hawaii Ocean Time-series (HOT) program. The resulting data reveal that particulate matter concentrations are maximal and relatively homogenous throughout the upper water column ( $< 75 \text{ m}$ ) before declining steeply toward the lower portion of the euphotic zone ( $\sim 75$  to  $175 \text{ m}$ ) [Hebel and Karl, 2001]. However, the relatively coarse sampling resolution of these measurements in space and time (nine depths in the upper 200 m at nearly monthly intervals) limits our understanding of the physical and biological processes that structure particulate matter distributions in this region. Furthermore, while bulk elemental composition measurements provide important information on inventories and stoichiometry of particulate matter, such measurements do not include information on particle size, a characteristic influencing plankton metabolic rates [Brown *et al.*, 2004] and particle settling velocities [Smyda, 1970].

The particle size distribution (PSD) in seawater results from the local balances among numerous physical and biological processes, including plankton species composition and their growth rates, trophodynamic interactions (e.g., grazing and viral lysis), sinking rates, physical mixing, aggregation, and disaggregation [Burd and Jackson, 2009]. Arguably, the size and abundance of various taxa of phototrophic organisms are

among the most important factors influencing the PSD. Phytoplankton mediate the transformation of inorganic substrates into particulate organic matter and thus represent an important control on particle dynamics. Moreover, physical processes, such as changes in stratification and turbulent mixing, can also influence the distribution of particles in the seawater. For example, particle maxima have been observed in layers of steep gradients in seawater density, presumably reflecting decreased settling speed of porous particles [Kindler *et al.*, 2010] or vertical heterogeneity of turbulent mixing [Macintyre *et al.*, 1995].

The aims of the current study were to characterize daily-scale variability in the particle size distribution at Station ALOHA during the summer of 2012 and to assess the extent to which vertical patterns in the PSD reflected changes in the physical and microbial characteristics of this habitat. To this aim, we adopted an optical method based on the use of in situ laser diffraction technology to reconstruct the size distribution of particles between 1.25 and 100  $\mu\text{m}$  in equivalent spherical diameter. This approach has been previously used with suspensions of microspheres of known size [Agrawal and Pottsmith, 2000], phytoplankton cultures [e.g., Rienecker *et al.*, 2008], and in other natural environments [e.g., Kostadinov *et al.*, 2012]. Moreover, the PSD obtained using laser diffraction has been previously compared to other particle sizing methods, including those based on electrical impedance (i.e., Coulter Counter) [Reynolds *et al.*, 2010; Buonassissi and Dierssen, 2010]. The laser diffraction methodology relies on measurements of the volume scattering function at near-forward angles that are interpreted on the basis of Mie theory to obtain the PSD [Agrawal and Pottsmith, 2000], generally under the assumption that particles are spherical. Given that size is not measured directly and that the procedure requires an assumption of particle shape, laser diffraction measurements provide a proxy of the true PSD, not unlike chlorophyll fluorescence provides a proxy for chlorophyll concentration [Lorenzen, 1966] or beam attenuation provides a proxy for total particle load [Jones and Wills, 1956]. Methodological limitations of the laser diffraction approach are counterbalanced by the ability to obtain high vertical and temporal resolution in situ measurements of the PSD, without complications introduced through water sampling and subsequent manipulation.

To ease the description of size spectra, it is useful to rely on simple mathematical functions that approximate the shape of the measured PSD. In the past, several authors proposed the use of a power law function to fit the PSD in aquatic environments [Bader, 1970; Stramski and Kiefer, 1991; Boss *et al.*, 2001]. The negative exponent of the fitted power law, also referred to as the PSD slope, reflects the relative importance of small particles compared to larger particles, and its value tends to be large in oligotrophic environments ( $>3.5$ ) [Buonassissi and Dierssen, 2010], where small particles are dominant. Given the simplicity of the power law function, its exponent could represent a useful metric to compare the shape of the PSD across environments and over time, but care should be taken to make sure that the variability in the estimates of this parameter does not derive from the use of different fitting procedures. To this aim, it is useful to identify which fitting choices affect the estimates of the PSD slope, so that a common procedure can be adopted in different investigations and environments.

Here we provide recommendations for collection and interpretation of forward scattering measurements in an optically clear environment such as Station ALOHA, and more significantly, we compare the retrievals of distinct particle size classes to phytoplankton cell concentrations, diagnostic pigments, beam attenuation as a proxy for particle load, and traditional measures of PC in an effort to characterize the nature of particles detected by laser diffraction in this environment. Furthermore, we test the utility of using a power law parameterization as a metric to compare different PSDs. Finally, in an attempt to explain the vertical variability of particle concentrations, we compare our observations of the PSD with the vertical position of selected features in the euphotic zone: the base of the mixed layer ( $Z_{ML}$ ), the depth of maximal stratification ( $Z_{MS}$ ), and the depth of the chlorophyll *a* maximum ( $Z_{CM}$ ).

## 2. Material and Methods

The measurements conducted in this study were made between July and September of 2012, during three oceanographic cruises that were part of the HOE-DYLAN (Hawaii Ocean Experiment—Dynamics of Light And Nutrients) expeditions to Station ALOHA. These cruises spanned 9–25 July, 6–13 August, and 23 August to 8 September. The overall objective for this large-field effort was to evaluate daily to monthly scale variability in physical and biogeochemical dynamics via high-frequency sampling of the upper ocean. The HOE-DYLAN expeditions included daily deployments of a bio-optical package and the collection of seawater

samples at discrete depths every 3 days around 4 P.M. (for a total of 11 vertical profiles) using 12 L sampling bottles to measure PC and phytoplankton pigments, and to enumerate picoplankton cell abundances by flow-cytometric analysis. The vertical layer of interest for this study was the euphotic zone, defined as the depths above the compensation irradiance, or 0.11% of the downwelling photosynthetically available radiation incident at the sea surface [Laws *et al.*, 2014]. The depth of the euphotic zone during the HOE-DYLAN expedition was estimated using a hyperspectral radiometer and reached a maximum depth of 164 m. In this study, we extended our analyses to a constant depth horizon of 180 m in order to use a conservative criterion that always included the euphotic zone in its entirety.

## 2.1. Bio-Optical Package Deployments

Daily vertical profiles of the upper 200 m were obtained using an in situ bio-optical package including a chlorophyll fluorometer (WET Labs, excitation/emission: 470/695 nm), a particle size analyzer (LISST 100X type-B, Sequoia Scientific, hereafter LISST), an in situ spectrophotometer (ac-s, WET Labs), and a CTD (conductivity, temperature, and depth) package (SBE37, Sea-Bird). A total of 39 deployments of the bio-optical package were performed during the three HOE-DYLAN cruises. All deployments occurred at night and consisted of two consecutive casts to  $\sim 210$  m at a constant descent velocity of  $10 \text{ m min}^{-1}$ . After reaching the target depth, the package was held for 1 min before raising it back to the sea surface at an ascent velocity of  $10 \text{ m min}^{-1}$ .

## 2.2. Particle Size Distribution

The volume scattering function at near-forward angles was measured with the LISST on 32 ring detectors arranged as to intercept light scattered at 32 different angles from a collimated laser beam (emission  $\lambda = 670 \text{ nm}$ ). Using Mie theory, the distribution of the light scattered was inverted to obtain the volumetric particle concentration [Agrawal and Pottsmith, 2000] in 32 logarithmically spaced size classes ranging in diameter from 1.25 to  $250 \mu\text{m}$  (bin limits at  $1.25 \times 1.801^n \mu\text{m}$ , with  $n = 0, 1, 2, \dots, 32$ ). The scattering inversion was performed using the kernel matrix provided by the instrument's manufacturer (Sequoia Scientific) for analyses of spherical particles. This kernel was chosen based on the results of a comparative analysis of the PSDs reconstructed using three different kernel matrices at Station ALOHA (A. E. White *et al.*, manuscript in preparation, 2015).

Prior to deriving the particle volume distribution, the background scattering attributable to water was subtracted from the measured LISST signal. For this correction we evaluated two different approaches: (1) we measured the scattering by deionized water onboard the ship prior to the deployment of the instrument; and (2) we isolated the signal measured by the LISST at the bottom of each cast (between 202 and 204 m). For consistency, and because deep water values were at times lower than that of deionized water (no significant difference with a one-tailed *t* test, average  $p = 0.90$  over the 32 rings,  $n = 7$ ), we chose to use the deep water as the background reference. This choice allowed us to associate a background scattering with each downcast, accounting for cast-to-cast changes in instrument performance. Furthermore, this approach assumes that the variability in the measurements of light scattered at 202–204 m is due to changes in the performance of the optical sensor and that particle concentration at this depth and deeper in the water column is below the limit of detection of the instrument. Even though the LISST cannot detect particles at  $\sim 200$  m, PC is still measurable at this depth, averaging  $0.7 \mu\text{mol L}^{-1}$  in the summer 2012. Although some fraction of this material likely falls into the size range detected by the LISST, its scattering signal is below the detection limit of our instrument.

After performing the scattering inversion for each bio-optical cast, the average particle volume distributions were computed at 2 m intervals, and the resulting volume distributions (in units of  $\mu\text{L L}^{-1}$ ) from the two consecutive downcasts were averaged to obtain a single daily vertical profile. Volume distribution on each 2 m bin was an average of  $\sim 240$  LISST scans and corresponded to a scanned volume of 0.4 L. Values from the volumetric concentration that were more than three standard deviations from the mean within a 2 m vertical bin were excluded (2% of the measurements). Particle size distributions were computed by dividing the volumetric concentrations at each size bin by the volume of the sphere,  $V$ , with a diameter equal to the geometric mean diameter of the bin. Normalized abundances (particles  $\text{L}^{-1} \mu\text{m}^{-1}$ ) were obtained by scaling the abundances by the width of the bin. To transform particle abundances into particulate carbon concentrations, we used the relationship derived by Menden-Deuer and Lessard [2000]:

$$C = 0.216 \times V^{0.939} \quad (1)$$

where  $C$  is the carbon content of a particle (pg C), and  $V$  is its volume ( $\mu\text{m}^3$ ). Then, we multiplied  $C$  from each of the 32 bins to the respective particle abundance to obtain estimates of PC within each size bin.

One of the challenges in employing laser diffraction to enumerate particles in oligotrophic environments stems from the low signal-to-noise in particle scattering [Andrews *et al.*, 2011]. In addition, the derivation of PSD from laser diffraction is sensitive to sunlight [Andrews *et al.*, 2011], scattering due to gradients in sea-water density [Styles, 2006; Mikkelsen *et al.*, 2008], and the presence of air bubbles close to the sea surface [Stramski and Tegowski, 2001]. To address these issues, we follow these guidelines: (1) all casts were conducted at night in order to avoid complications related to sunlight; (2) we exclude the five largest size bins (109–250  $\mu\text{m}$ ) from our analyses to exclude scattering as a result of density gradients, which affects the bins bigger than  $\sim 100$   $\mu\text{m}$  [Styles, 2006]; and (3) we limited our analysis to depths greater than 20 m to exclude the potential influence of air bubbles on the PSD; the presence of bubbles was apparent as a substantial increase in particle volume at shallow depths ( $< 20$  m, data not shown) that was independent of changes in measured PC concentrations. Restricting our analyses to depths  $> 20$  m was likely a conservative criterion given that wind speeds observed during our cruises were  $< 11$   $\text{m s}^{-1}$  from which we estimate bubble penetration depths of  $< 15$  m [Vagle *et al.*, 2010].

To simplify the description of size spectra, we grouped 27 discrete LISST size bins into three size classes. In defining the size classes, we adopted the threshold values proposed by Sieburth *et al.* [1978] for the separation of planktonic organisms in to picoplankton (0.2–2  $\mu\text{m}$ ), nanoplankton (2–20  $\mu\text{m}$ ), and microplankton (20–200  $\mu\text{m}$ ). Consequently, we grouped the first three LISST bins (effective size range of 1.25–2.05  $\mu\text{m}$ ) and refer to them as 1.25–2  $\mu\text{m}$  particles; LISST bins 4–17 (effective size 2.05–20.9  $\mu\text{m}$ ) are referred to as 2–20  $\mu\text{m}$  particles; and LISST bins 18–27 (effective size 20.9–109  $\mu\text{m}$ ) are referred to as 20–100  $\mu\text{m}$  particles. We define the total particle volume (TPV,  $\mu\text{L L}^{-1}$ ) as the sum of the volumetric concentration of these three size classes. TPV represents an optical proxy for particle load in the 1.25–109  $\mu\text{m}$  range.

### 2.3. Power Law Parameterization

The formulation of the power law model that we used to approximate the PSD is:

$$n(D) = n_0 \left( \frac{D}{D_0} \right)^{\xi} \quad (2)$$

where  $n$  (particles  $\text{L}^{-1} \mu\text{m}^{-1}$ ) is the particle concentration normalized by the bin width,  $D$  ( $\mu\text{m}$ ) is the diameter of the particles,  $D_0$  ( $\mu\text{m}$ ) is a reference diameter,  $n_0$  (particles  $\text{L}^{-1} \mu\text{m}^{-1}$ ) is the normalized abundance at  $D_0$ , and  $\xi$  is the exponent of the power law. Approximating the PSD with this model requires the selection of a size range where the model is assumed to apply, and the choice of a fitting algorithm that reflects the distribution of the error within the estimated PSD. Previous studies using laser diffraction [Reynolds *et al.*, 2010; Buonassissi and Dierssen, 2010; Kostadinov *et al.*, 2012] excluded the smallest size bins in their computation of the PSD exponent because this region of the size spectrum is highly sensitive to deviations from sphericity and to ambient light [Andrews *et al.*, 2011]. The same studies used a linear regression model on log-transformed data for power law curve fitting; however, this method is known to produce systematically biased estimates of parameters for power laws [Clauet *et al.*, 2009]. To assess the viability of using power law parameterizations to compare the shape of the PSD from different environments, we calculated the difference among the exponent of the power law obtained on different size ranges and by using two alternative fitting algorithms. Such analysis provided information on the sensitivity of the power law parameterization to the particle size range and to the curve fitting procedures.

The curve fitting algorithms used to compute the power law exponent of the PSD were: (1) weighted non-linear least squares, where the weight assigned to each bin was represented by the inverse of the variance measured in that bin; (2) a linearized power law model involving a linear regression on log-transformed data (dependent and independent variables). The main difference between the two methods is that the linearized model relies on the assumption of constant error variance (in log space) with particle size, while the weighted least squares method uses the bin variance to estimate the error variance for different particle size. Curve fitting was also performed on different size ranges to test the effect of the inclusion of the smallest size bins in the computation of the power law exponent (while keeping 109  $\mu\text{m}$  as the upper size limit).

The lower limits of the size range were selected based on those used in three previous studies [Reynolds *et al.*, 2010; Buonassissi and Dierssen, 2010; Kostadinov *et al.*, 2012] that computed exponents of the power law on PSD based on laser diffraction. Weighted least squares minimization was performed in MATLAB using the `lsqnonlin` function in the optimization toolbox.

#### 2.4. Particulate Carbon, Cell Abundances, and Pigment Concentrations

Water samples for determinations of PC concentrations were collected from eight discrete depths (5, 25, 45, 75, 100, 125, 150, and 175 m) and prefiltered through 202  $\mu\text{m}$  Nitex mesh; subsequently 4 L were pressure filtered through combusted 25 mm GF/F glass fiber filters (nominal porosity 0.7  $\mu\text{m}$ ). Filters were frozen ( $-20^{\circ}\text{C}$ ) in cleaned Petri dishes until shore-based analysis. Three combusted 25 mm GF/F glass fiber filters were also frozen in cleaned Petri dishes for PC blank determination to account for background carbon concentration on filters before filtration. In the laboratory, filters were dried and pelleted, and PC concentrations were measured by combustion using an Exeter Analytical CE-440 CHN elemental analyzer (Exeter Analytical, UK). The samples were combusted in pure  $\text{O}_2$  and the combustion by-products ( $\text{CO}_2$ ,  $\text{H}_2\text{O}$ , and  $\text{N}_2$ ) were measured with a series of high-precision thermal conductivity detectors. The filter blank value corresponded to a concentration of  $0.33 \pm 0.07 \mu\text{mol C L}^{-1}$  (considering a filtered volume of 4 L) that was subtracted from the total filtered sample PC concentration.

Abundances of both pigmented and nonpigmented plankton were quantified by flow cytometry on a volume of 100  $\mu\text{L}$ . Seawater for these analyses was collected in 2 mL cryovials and preserved with microscopy-grade paraformaldehyde (0.24% vol/vol final concentration) from the same depths sampled for PC. Cells were fixed for 15 min in the dark prior to flash freezing in liquid nitrogen, then stored at  $-80^{\circ}\text{C}$  until analysis. Pigmented cells (*Prochlorococcus*, *Synechococcus*, and pigmented eukaryotes) were enumerated with an Influx (Becton-Dickson) flow cytometer using two excitation lasers (457 and 488 nm) to stimulate chlorophyll and phycoerythrin fluorescence, respectively. Nonpigmented picoplankton were enumerated from SYBR I stained cells (Life Technologies) and cell abundances were determined following subtraction of *Prochlorococcus* abundances from the total SYBR-positive cell abundances.

Cell abundances were converted to carbon using a single conversion factor for each cell population: conversion factors for *Prochlorococcus* and *Synechococcus* were 36 and 255 fg C cell $^{-1}$  [Buitenhuis *et al.*, 2012], respectively, and 6.3 fg C cell $^{-1}$  was applied to the nonpigmented picoplankton [Kawasaki *et al.*, 2011]. These are approximate estimations of the carbon content of cells, actual cell specific carbon is known to vary. For example, Buitenhuis *et al.* [2012] report a threefold variation of the conversion factors with depth for both *Prochlorococcus* and *Synechococcus*.

The concentrations of chlorophyll *a* (monovinyl + divinyll forms), chlorophyll *b* (monovinyl + divinyll forms), chlorophyll *c*, and photosynthetic carotenoids (fucoxanthin, 19'-hexanoyloxyfucoxanthin, and 19'-butanoyloxyfucoxanthin) were measured by high-performance liquid chromatography (HPLC) following the procedures described in Bidigare *et al.* [2005]. Seawater samples were collected daily at 25 m and at  $Z_{\text{CM}}$ , and every 3 days at the same eight discrete depths where PC and cell abundances were measured. Two to four liters of water were filtered for pigment analysis.

#### 2.5. Hydrography, Chlorophyll Fluorescence, and Beam Attenuation

Temperature, salinity, and chlorophyll fluorescence were binned into 2 m intervals by averaging measurements from the two downcasts conducted on each deployment of the bio-optical package. Beam attenuation at a wavelength of 648 nm,  $c$ , was measured with an ac-s and binned into 2 m intervals using measurements from only one of the two upcasts of each deployment of the bio-optical package. Upcast measurements were utilized for the beam attenuation to reduce the potential interference from air bubbles trapped in the flow chamber of the ac-s during the downcast. Furthermore, one of the two casts was used to measure beam attenuation attributable to dissolved substances in the seawater, so it could not be used for the purpose of this study. Beam attenuation measurements are sensitive to abrupt changes in the particle field, for example, the passage of large zooplankton through the light beam [Bishop and Wood, 2008]. For this study, these transient spikes were excluded by prebinning data on a 20 m vertical grid and by removing those values that differed more than three standard deviations from the 20 m bin average. Temperature and salinity were used to compute potential density,  $\rho$ , that was used to calculate the depth at the base of the mixed layer,  $Z_{\text{ML}}$ , as the first depth where the potential density was at least  $0.03 \text{ kg m}^{-3}$  larger than the value at 10 m [de Boyer Montégut *et al.*, 2004].

We used the Brunt-Väisälä frequency,  $N$ , as an index of the stability of the water due to stratification.  $N$  was calculated as:

$$N = \sqrt{-\frac{g}{\rho} \frac{\partial \rho}{\partial z}} \quad (3)$$

where  $g$  is the gravitational acceleration,  $z$  is the depth, and the potential density vertical gradient,  $\partial \rho / \partial z$ , was computed by the central finite difference method. The depth of maximal stratification,  $Z_{MS}$ , and the maximum value of  $N$  were calculated for each profile in the 20–150 m depth range.

The depth of the chlorophyll  $a$  maximum,  $Z_{CM}$ , was computed on profiles of calibrated fluorescence. Several photosynthetic pigments can absorb light emitted by the fluorometer at 470 nm, and transfer the excitation energy to the reaction center of photosystem II where it is reemitted as fluorescence. To take into account the role of pigments other than chlorophyll  $a$  in this process, fluorescence was converted into units of chlorophyll  $a$  concentration in two steps: (1) applying a linear transformation ( $R^2 = 0.86$ ) based on the regression between fluorescence and the cumulative concentration of photosynthetic pigments measured by HPLC (chlorophyll  $a$  + chlorophyll  $b$  + chlorophyll  $c$  + photosynthetic carotenoids); and (2) converting photosynthetic pigment concentration into chlorophyll  $a$  by using a depth-dependent ratio of chlorophyll  $a$ : photosynthetic pigments. The depth-dependent ratio of chlorophyll  $a$ : photosynthetic pigments was computed by fitting a sigmoidal curve (Gompertz function,  $R^2 = 0.93$ ) to the ratios of these pigment concentrations during the three cruises of this study.

Beam attenuation due to pure water,  $c_w$ , was estimated on deck by measuring the attenuation of deionized water. Twelve measurements of  $c_w$  were used to construct a linear regression for the time period of this study to track the drift of instrument performance over time. From the linear model, we obtained a  $c_w$  for each cast, and we subtracted its value from the total beam attenuation to isolate the signal due to material suspended in the seawater.

### 3. Results

#### 3.1. Detection of Forward Angle Scattering at Station ALOHA

The signal measured at the 32 ring detectors of the LISST was compared to the background signal collected in deep water (202–204 m) to test the statistical significance of particle scattering. Comparisons were performed for single downcasts after scaling to account for changes in the power of emitted light [Agrawal and Pottsmith, 2000], and results were analyzed together to assess the percent of statistically significant values on 2 m vertical bins (Figure 1a). Scattering at larger angles (associated with greater ring numbers) was significantly different from the background more frequently than scattering at smaller angles. In particular, the outermost rings of the LISST (rings 12–32) were significantly different from the background in the 20–150 m vertical layer in >90% of samples (one-tailed, two-samples  $t$  test  $p < 0.05$ , Figure 1a). Conversely, the innermost four rings were often (>50%) not significantly different from the background in the 20–200 m vertical layer. Rings 5–11 were characterized by a decrease in significance with depth and by an average increase in significance with ring number. Considering that smaller particles tend to scatter light at larger angles, we find that the LISST signal in this system is largely driven by scattering from particles having an equivalent spherical diameter of 1.25–40  $\mu\text{m}$  (measured by rings 12–32). On average, these particles accounted for more than 90% of TPV in the 20–180 m layer (Figure 1b).

#### 3.2. Mixed Layer, Stratification Maximum, and Pigment Variability

The average position of the base of the mixed layer was  $41 \pm 14$  m ( $\pm$  symbol precedes standard deviation throughout the manuscript) with deeper mixing in the early part of this study ( $Z_{ML} = 72$  m on 13 July, Figure 2a). The average depth of maximal stratification,  $Z_{MS}$ , was  $72 \pm 15$  m and was characterized by an average Brunt-Väisälä frequency of  $0.02 \text{ s}^{-1}$ .  $Z_{CM}$  occurred deeper in the euphotic zone ( $121 \pm 10$  m); part of the variability in the vertical position of this feature was likely due to the vertical movement of isopycnal layers consistent with displacement by internal waves in this region [Merrifield *et al.*, 2001]. Chlorophyll  $a$  concentrations from calibrated fluorescence ranged from 63 to 131  $\text{ng L}^{-1}$  in the mixed layer and increased with depth to maximum values of 257–355  $\text{ng L}^{-1}$  (Figure 2a). Mixed-layer chlorophyll  $a$  was particularly elevated during 13–15 July with concentrations averaging  $124 \pm 7 \text{ ng L}^{-1}$  and was significantly greater (one-tailed, two-samples  $t$  test  $p = 5 \times 10^{-5}$ ) in mid- to late-July than in August–September. Fucoxanthin

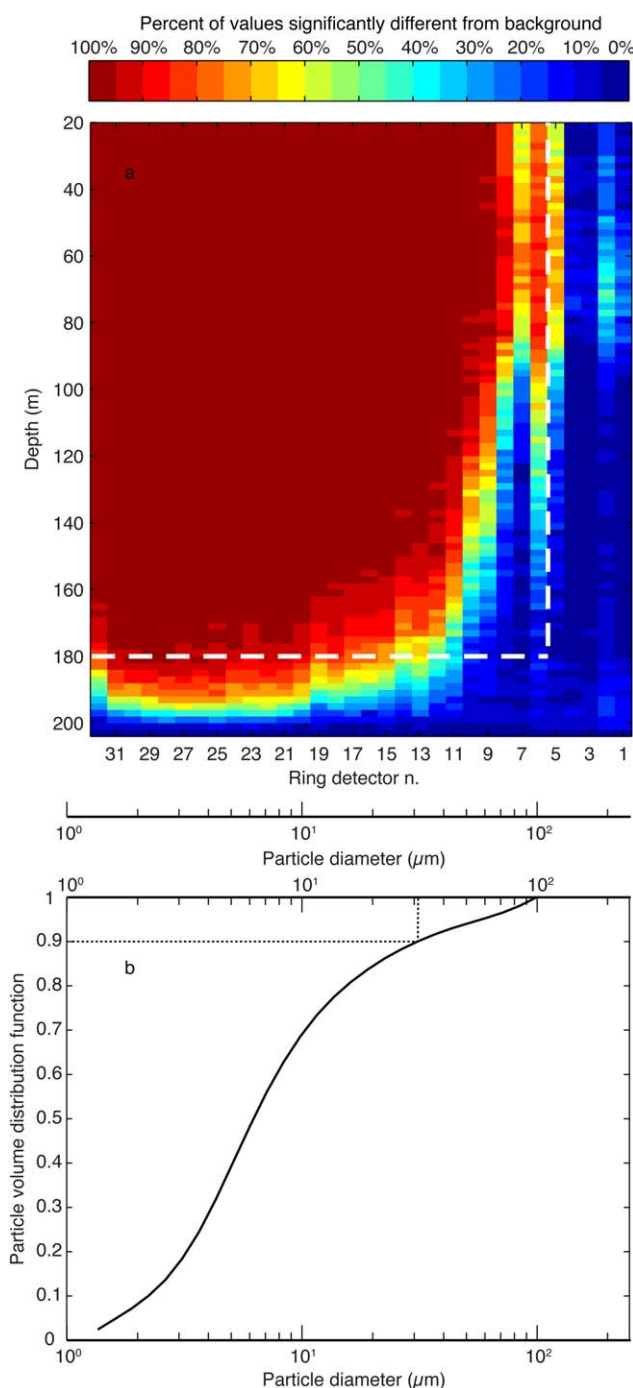


**Figure 1.** (a) Percent of LISST raw measurements significantly different from the background (one-tailed  $t$  test, for  $p < 0.05$ , data are scaled to account for variations of laser power). The  $x$  axis represents both the number of the ring detector and the size of particles that most effectively scatter light at that angle. Dashed white lines define the depth range and the particle size range considered in this study. (b) Cumulative distribution function of particle volume, depicting the fraction of TPV contained in particles smaller than the size on the  $x$  axis. The distribution is an average of all measurements in the 20–180 m depth range. Dotted line marks the upper limit of the particle size range containing 90% of TPV.

Particles ranging in size between 20 and 100  $\mu\text{m}$  tended to have lower volumetric concentrations, with volumes elevated and most variable throughout the upper 80 m, and decreasing with depth. The contribution of 1.25–2  $\mu\text{m}$  particles to TPV was smaller than the other two size classes; this particle size range displayed

concentrations at 25 m averaged  $5.0 \pm 1.3 \text{ ng L}^{-1}$  and were also significantly greater ( $p = 7 \times 10^{-7}$ ) in mid- to late-July when compared to those observed later in the summer ( $5.8 \pm 1.0$  versus  $4.5 \pm 1.1 \text{ ng L}^{-1}$ ).

### 3.3. Vertical and Temporal Variability of TPV and Beam Attenuation

Throughout the summer, TPV was consistently elevated between 20 and 80 m ( $0.076 \pm 0.014 \mu\text{L L}^{-1}$ ), decreasing with depth into the lower regions of the water column (Figure 2b). TPV often increased near the base of the mixed layer. A notable exception occurred on 13 July when TPV was elevated ( $0.11 \pm 0.01 \mu\text{L L}^{-1}$ ) throughout the surface mixed layer. This feature evolved with time, forming a maximum volumetric concentration ( $0.16 \mu\text{L L}^{-1}$ ) close to the base of the mixed layer on 14 July. In the mixed layer, TPV was elevated in mid-July and depressed in September. From 23 August to 7 September, we measured a continuous decrease in mixed-layer TPV that coincided with an intrusion of low-salinity water (mixed-layer salinity decreased by 0.38 during the last 2 weeks of the study period).

Temporal and vertical variability in beam attenuation resembled the variability observed in TPV (Figures 2b and 2c), and the two parameters were strongly correlated during the study period ( $R^2 = 0.83$ ,  $n = 3159$ ).

### 3.4. Vertical Distribution of Different Size Fractions

Binning the 27 particle size classes measured by the LISST into three major size classes (1.25–2, 2–20, and 20–100  $\mu\text{m}$ ) provided information on the vertical structure of particles in the upper ocean at Station ALOHA (Figure 3). Particles in the 2–20  $\mu\text{m}$  size range were the dominant contributors to TPV (averaging  $77 \pm 12\%$ ) between 20 and 180 m, with peak volumetric concentrations occurring at  $54 \pm 17 \text{ m}$ .

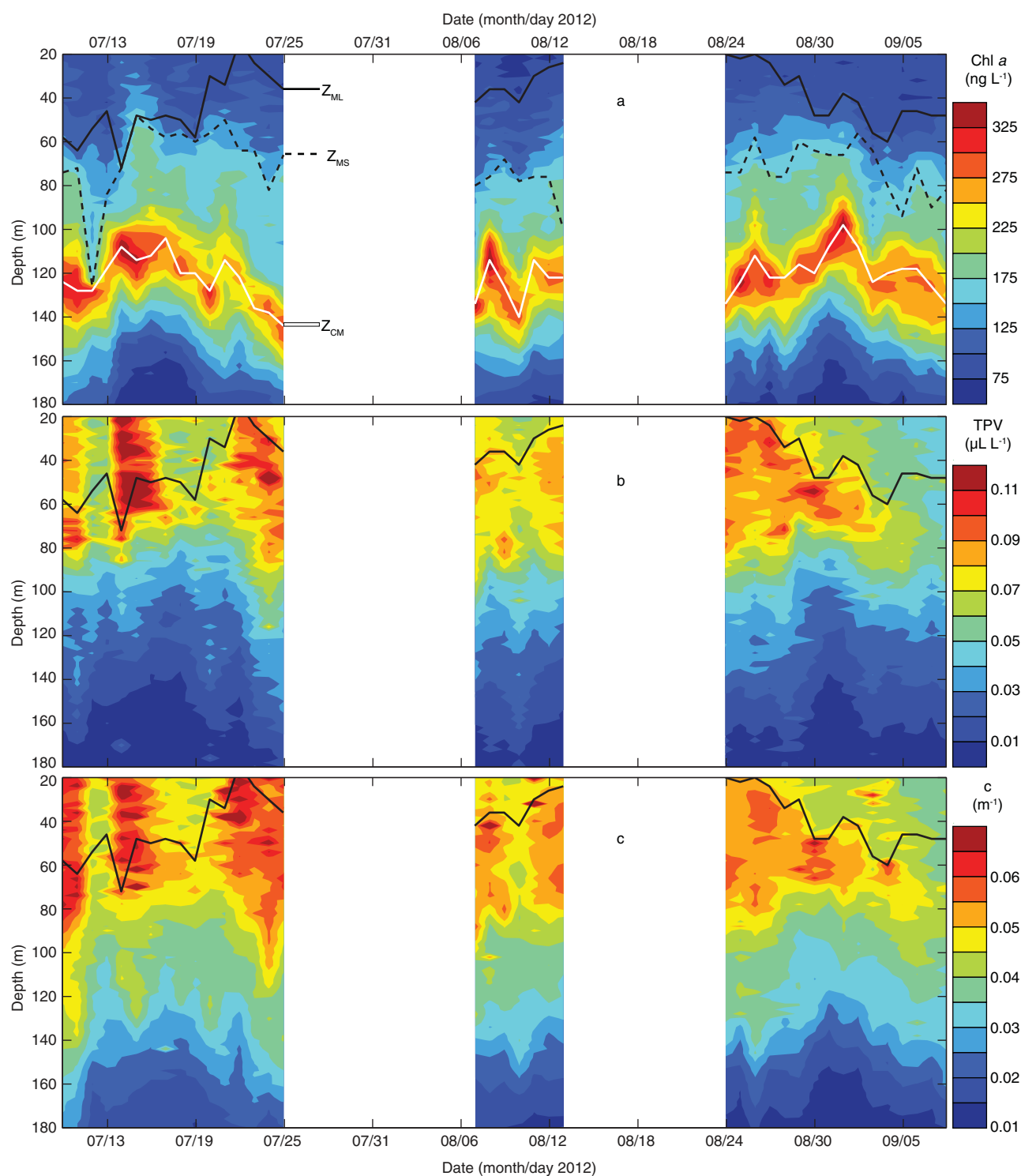


**Figure 2.** Temporal variability during the three HOE-DYLAN cruises associated with (a) Chlorophyll *a* from calibrated fluorescence; (b) TPV (note that the color scale does not capture the 13–15 July event where the volumetric concentration reached values of  $0.17 \mu\text{L L}^{-1}$ ); and (c) beam attenuation at a wavelength of 648 nm. The depth of the base of the mixed layer ( $Z_{ML}$ ) is depicted as a solid black line in Figures 2a–2c; the dashed black line in Figure 2a depicts the depth of the maximum of the Brunt-Väisälä frequency ( $Z_{MS}$ ); the solid white line in Figure 2a depicts the depth of the deep chlorophyll *a* maximum ( $Z_{CM}$ ).

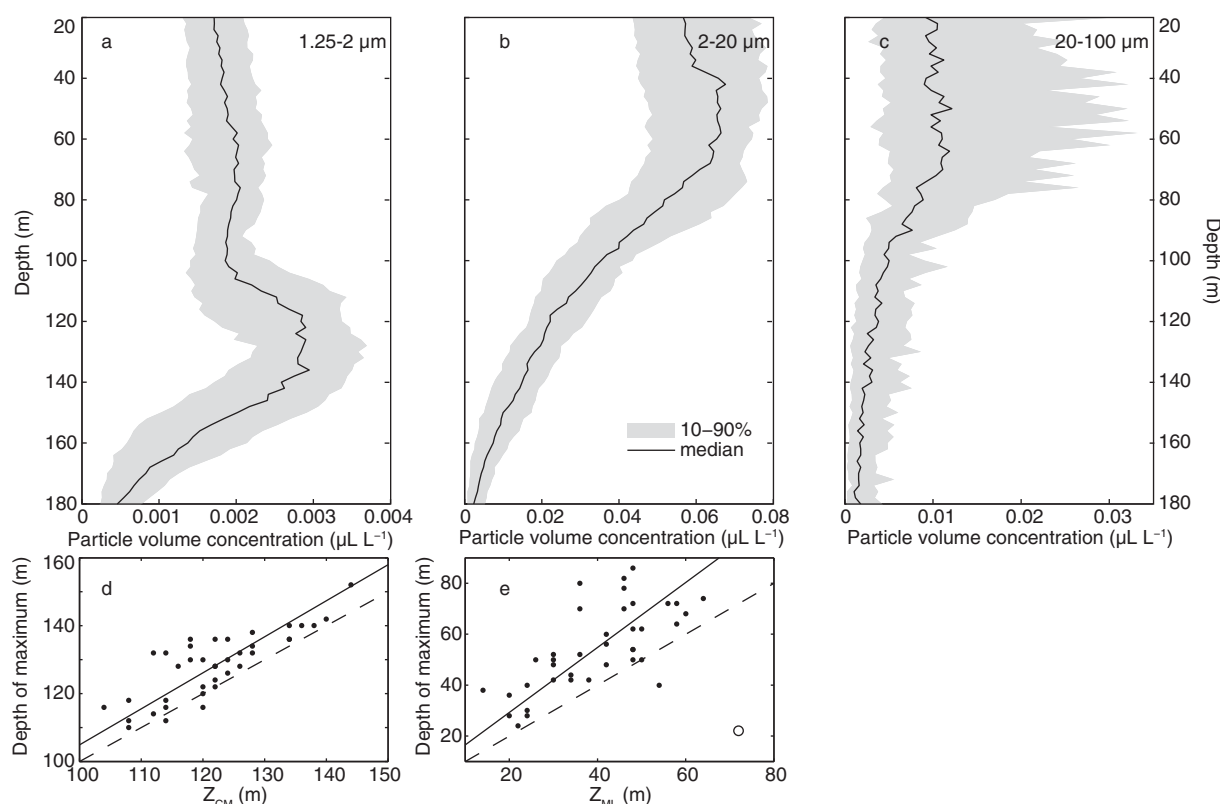


**Figure 3.** Vertical profiles of the particle volumetric concentration in three size classes: (a) 1.25–2  $\mu\text{m}$ , (b) 2–20  $\mu\text{m}$ , and (c) 20–100  $\mu\text{m}$ . Solid lines are median values and gray areas include values between the tenth and the ninetieth percentiles. (d) Depth of the 1.25–2  $\mu\text{m}$  particle maximum versus  $Z_{CM}$  (symbols are observations, the solid line is the geometric mean regression, and the dashed line is the 1:1 line); (e) depth of the 2–20  $\mu\text{m}$  particle maximum versus  $Z_{ML}$  (symbols and lines as in Figure 3d with the open circle depicting one data point excluded from the regression analysis).

maximal volume between  $\sim 110$  and 150 m, encompassing the  $Z_{CM}$ . In contrast, the volume of 2–20  $\mu\text{m}$  particles appeared relatively constant through the upper 80 m, declining sharply with increasing depth between 80 and 180 m.

Least squares linear regression analyses were used to examine the relationships between the depth of the particle volume maxima for the various size-fractions and the  $Z_{ML}$ ,  $Z_{MS}$ , and  $Z_{CM}$  depths (Table 1). In addition, the mean distances,  $\Delta z$ , of the particle maxima from  $Z_{ML}$ ,  $Z_{MS}$ , and  $Z_{CM}$  were computed (Table 1). These analyses revealed a significant relationship between the depth of the maximum of 1.25–2  $\mu\text{m}$  particles and  $Z_{CM}$  (Figure 3d); on average,  $Z_{CM}$  was 4 m shallower than the depth of the particle maxima for these small particles. In contrast, the depths of the maxima of both 2–20  $\mu\text{m}$  particles (Figure 3e) and TPV was associated to  $Z_{ML}$  with particle maxima on average 14 m deeper than the base of the mixed layer. In all of these relationships, the slopes of the linear regressions were close to unity (Table 1), implying that vertical variations in the depth of particle maxima were associated with equivalent vertical variations in the associated feature (either  $Z_{ML}$  or  $Z_{CM}$ ).

We observed that the abundance of particles in the 1.25–2  $\mu\text{m}$  size range peaked at the depth of the chlorophyll *a* maximum; these particles were also the most abundant particles at depths  $> 100$  m within the size range quantified by laser diffraction (even if they were 2–3 orders of magnitude less abundant than bacterial cells in the entire water column). Based on flow cytometry cell counts, we observed that the maximum in 1.25–2  $\mu\text{m}$  particles coincided with the region in the euphotic zone where photosynthetic eukaryotic phytoplankton abundance was elevated (Figure 4). Moreover, the abundances of photosynthetic eukaryotes were statistically indistinguishable (two sample *t* test,  $p = 0.43$ ,  $n = 11$ ) from abundances of 1.25–2  $\mu\text{m}$  particles at all the discrete depth horizons sampled for flow cytometry.

### 3.5. Size Distribution of Particle Abundance and Particle Volume

The characteristic size distributions of particle abundance and particle volume are represented by the median spectra for both these properties within the mixed layer, and at  $Z_{CM}$  (Figures 5a and 5b). The

**Table 1.** Vertical Correlation Between Particle Maxima and Selected Layers<sup>a</sup>

	$Z_{ML}$			$Z_{MS}$			$Z_{CM}$		
	$R^2$	Slope	$\Delta z$	$R^2$	Slope	$\Delta z$	$R^2$	Slope	$\Delta z$
Depth max 1.25–2 $\mu\text{m}$	0.01	$-0.82 \pm 0.18$	88	<b>0.17</b>	$0.73 \pm 0.13$	58	<b>0.71</b>	$1.06 \pm 0.10$	4
Depth max 2–20 $\mu\text{m}$	<b>0.49</b>	$1.28 \pm 0.17$	14	0.03	$1.43 \pm 0.30$	–12	0.02	$1.68 \pm 0.36$	–64
Depth max 20–100 $\mu\text{m}$	0.03	$1.59 \pm 0.34$	18	0.06	$1.49 \pm 0.32$	–10	0.05	$2.07 \pm 0.43$	–62
Depth max TPV	<b>0.22</b>	$1.24 \pm 0.21$	14	0.00	$1.35 \pm 0.31$	–20	0.00	$1.63 \pm 0.37$	–70

<sup>a</sup>Results of Model II least squares linear regression analyses (geometric mean regression) of particle maxima and the depth of the chlorophyll *a* maximum ( $Z_{CM}$ ), the base of the mixed layer ( $Z_{ML}$ ), and the depth of maximum stratification ( $Z_{MS}$ ). The coefficient of determination,  $R^2$ , the slope of the linear regression, and the mean distance between the two depths,  $\Delta z$  (in meters) are shown. Coefficient of determination values in bold indicate those correlations significant at  $p < 0.01$  (Student's *t* test). One data point was excluded from the regressions versus  $Z_{ML}$ .

normalized abundance of 1.25–2  $\mu\text{m}$  particles increased with depth from an average of  $0.92 (\pm 0.31) \times 10^6$  particles  $\text{L}^{-1} \mu\text{m}^{-1}$  in the mixed layer to  $1.85 (\pm 0.52) \times 10^6$  particles  $\text{L}^{-1} \mu\text{m}^{-1}$  at  $Z_{CM}$  (Figure 5a). Particles 3–10  $\mu\text{m}$  in diameter contributed most to particle volume both in the mixed layer and at  $Z_{CM}$  (Figure 5b). While 3–10  $\mu\text{m}$  particles constituted  $56\% \pm 7\%$  of the TPV within the mixed layer, their contribution significantly decreased at depths  $>100$  m to become  $50\% \pm 4\%$  of the TPV at  $Z_{CM}$  (Figure 6a, *t* test  $p < 0.01$ ,  $n = 38$ ). Within this size class, particles 5–6  $\mu\text{m}$  in diameter were dominant components of TPV (Figure 6b). In contrast, despite their numerical importance, particles 1.25–2  $\mu\text{m}$  contributed the least to TPV accounting for  $2.0\% \pm 0.5\%$  of the TPV in the mixed layer, and increasing to  $10.2\% \pm 2.3\%$  at  $Z_{CM}$ . In waters deeper than 150 m, the contribution of 20–100  $\mu\text{m}$  particles to TPV increased.

### 3.6. Exponent of the Power Law Parameterization

Pure power law distributions are shaped as lines on log-log plots of particle size versus normalized particle abundance. A visual examination of the size distributions in Figure 5a reveals deviations from a pure power law, in particular for data collected within the mixed layer. Specifically, in the mixed layer, the decrease of

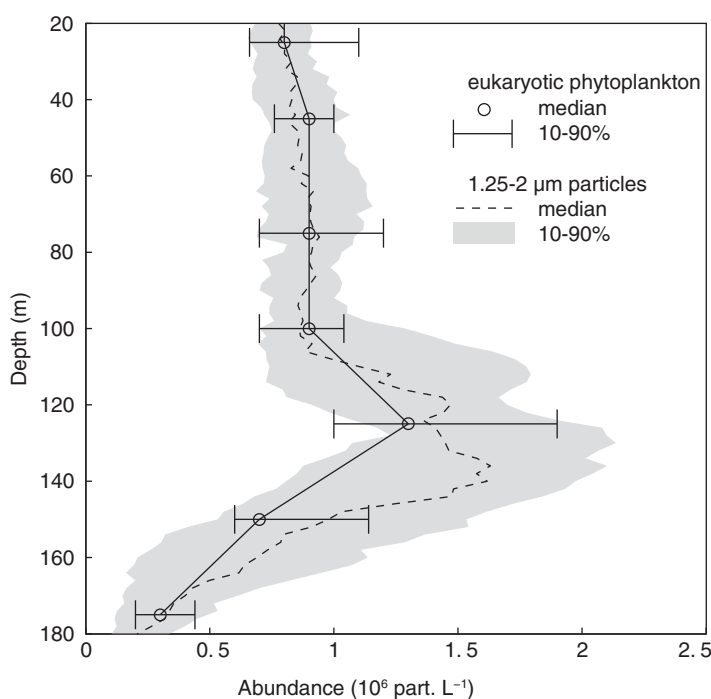


**Figure 4.** Profiles depicting the median vertical distributions of photosynthetic eukaryotes (solid line with bars) and the distribution of 1.25–2  $\mu\text{m}$  particles (dashed line and gray area). The bars and the gray area depict the tenth and the ninetieth percentiles of the respective profiles. Measurements shown include only those days when coincident measurements of both LISST-derived particle abundances and flow cytometric enumerations of photosynthetic eukaryotic plankton were obtained (11 discrete profiles in total).

particle abundance with size was more pronounced for particles  $>6 \mu\text{m}$  than for smaller particles. As a consequence, the exponent of the power law parameterization increased as the lower limit of the fitted size range increased (Table 2), both at  $Z_{CM}$  and within the mixed layer. The exponent was also greater when computed from a linearized model in all cases, aside from the most narrow size range (5.55–109  $\mu\text{m}$ ) on which the two algorithms gave very similar results. The average exponent at  $Z_{CM}$  was always greater than the same parameter computed within the mixed layer, but differences were only significant for some of the combinations of size ranges and fitting algorithms tested (Table 2).

### 3.7. Carbon Intercomparison

The median abundance of nonpigmented picoplankton

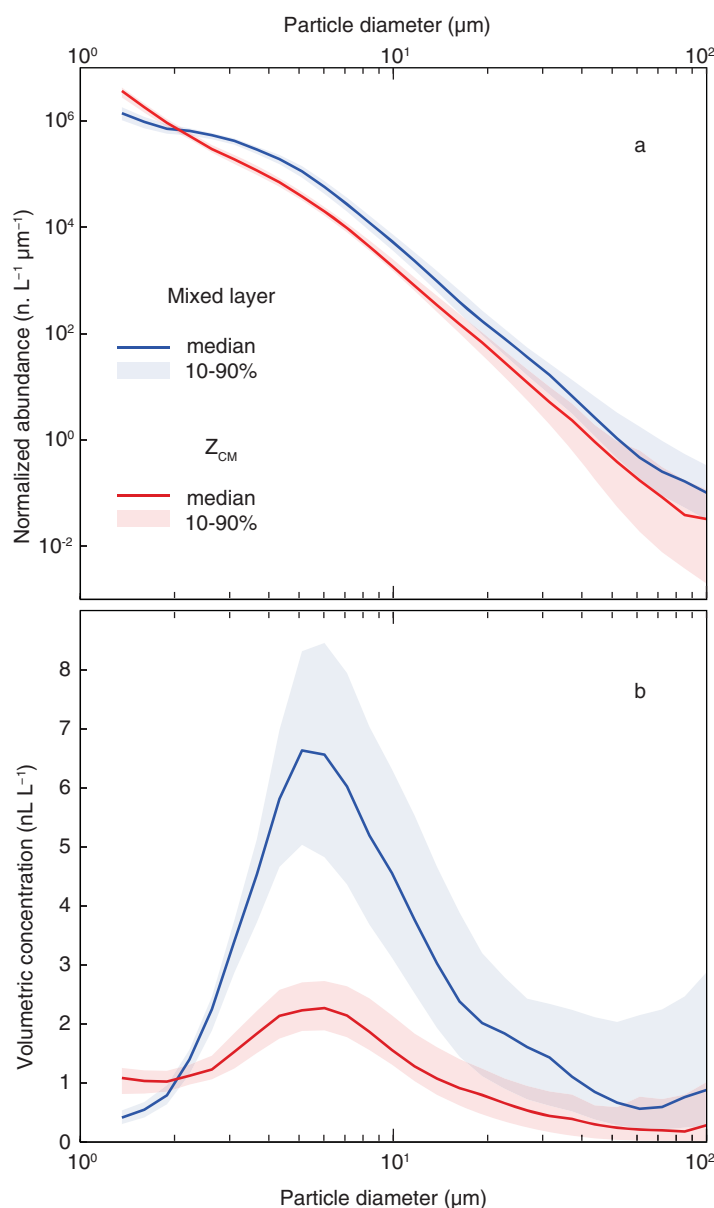


**Figure 5.** Median particle size spectra within the mixed layer and at  $Z_{CM}$ . (a) Spectra of particle abundance scaled by the width of the bin in  $\mu\text{m}$  and (b) spectra of particle volumetric concentration. Lines depict the median spectra, and areas include data between the tenth and the ninetieth percentiles.

bon associated with 1.25–100  $\mu\text{m}$  particles decreased with depth and was  $51\% \pm 14\%$  at 125 m, and  $27\% \pm 7\%$  at 175 m.

### 3.8. Temporal Variability of Different Size Fractions

In assessing temporal variability associated with the three particle size classes (1.25–2, 2–20, and 20–100  $\mu\text{m}$ ), we found that particles 1.25–2  $\mu\text{m}$  in size (Figure 8a) were most abundant at  $Z_{CM}$  during the entire period of our measurements. The concentrations of these particles within the mixed layer did not differ significantly among the three cruises (one-way ANOVA  $F_{2,37} = 0.13$ ,  $p = 0.88$ ). Temporal variability of 2–20  $\mu\text{m}$  particles (Figure 8b) resembled variability of TPV (Figure 2b). The volumetric concentration of 2–20  $\mu\text{m}$  particles in the mixed layer varied conspicuously within each of the three periods of our measurements, but did not differ significantly among the three separate cruise periods ( $F_{2,37} = 0.76$ ,  $p = 0.47$ ). The most

(including bacteria and archaea) was nearly constant throughout the upper 75 m, averaging  $5.6 (\pm 0.6) \times 10^5 \text{ cells mL}^{-1}$ , decreasing approximately two-fold through the lower euphotic zone. *Prochlorococcus* abundance averaged  $1.5 (\pm 0.3) \times 10^5 \text{ cells mL}^{-1}$  at 25 m, with abundances increasing to  $2.0 (\pm 0.3) \times 10^5 \text{ cells mL}^{-1}$  at 75 m before decreasing to  $0.7 (\pm 0.2) \times 10^5 \text{ cells mL}^{-1}$  at 125 m. The abundance of *Synechococcus* was consistently  $< 2.5 \times 10^3 \text{ cells mL}^{-1}$ . Conversion of cell and particle abundances to carbon concentrations indicates that the carbon in nonpigmented picoplankton + *Prochlorococcus* + *Synechococcus* (hereafter bacterial carbon) was maximal at 75 m, driven in large part by modest increases in *Prochlorococcus* abundance, and decreased with depth into the lower euphotic zone (Figure 7). Concentrations of both PC and 1.25–100  $\mu\text{m}$  particles also decreased below 75 m. Assuming that bacteria are too small to contribute to the LISST-derived 1.25–100  $\mu\text{m}$  particles, the sum of the flow cytometrically derived bacterial biomass and LISST-derived 1.25–100  $\mu\text{m}$  size fraction accounted for  $76\% \pm 9\%$  of measured PC between 25 and 75 m. The fraction of PC explained by bacterial carbon plus the car-

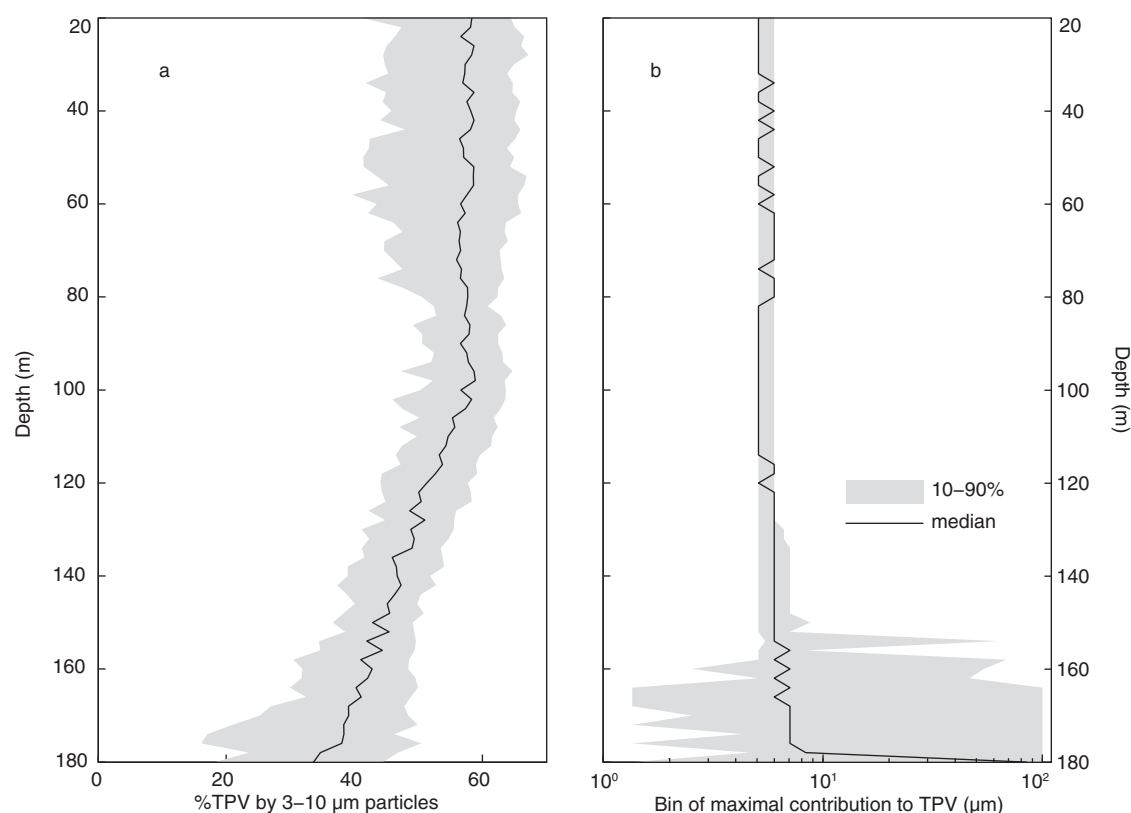


**Figure 6.** (a) Vertical profile of the percent contribution of the 3–10  $\mu\text{m}$  size fraction to TPV and (b) vertical profile of the size of the bin with the maximum particle volumetric concentration. In Figures 6a and 6b, solid lines represent median values and the gray area delimits the tenth and the ninetieth percentiles.

consistent variation was a continuous decrease in the average mixed-layer volume of 2–20  $\mu\text{m}$  particles by  $0.031 \mu\text{L L}^{-1}$  from 23 August to 7 September. The volume of 20–100  $\mu\text{m}$  particles within the mixed layer was significantly greater during July than during the other two sampling periods of this project (Figure 8c; one-way ANOVA  $F_{2,37} = 19.4$ ,  $p = 2 \times 10^{-6}$ , and Tukey-Kramer method). The average mixed-layer volume of 20–100  $\mu\text{m}$  particles was  $0.020 \pm 0.009 \mu\text{L L}^{-1}$  in mid-July, decreasing to  $0.008 \pm 0.003 \mu\text{L L}^{-1}$  in August–September. The greatest 20–100  $\mu\text{m}$  particle volume in the mixed layer was recorded during 13–15 July, and it was responsible for the abrupt change in TPV measured in the same time period. The large (greater than twofold within the mixed layer) decline in the abundance of 20–100  $\mu\text{m}$  particles between mid-July and early September coincided with a decrease in measured concentrations of the diatom pigment biomarker, fucoxanthin, in the upper ocean suggesting that the temporal decrease in particle size was related to a decrease in contribution of diatoms to phytoplankton biomass. Mixed-layer concentrations of fucoxanthin and the measured volume of 20–100  $\mu\text{m}$  particles displayed a positive correlation ( $R^2 = 0.24$ ,  $n = 38$ ,  $p < 0.05$ , Figure 9) providing support for the observation that variability in the particle size spectrum in the

**Table 2.** Exponent of the Power Law Within the Mixed Layer and at  $Z_{\text{CM}}$ <sup>a</sup>

Size Range ( $\mu\text{m}$ )	Weighted Nonlinear Model		Linearized Model		Lower Size Limit From
	$\zeta_{\text{ML}}$	$\zeta_{\text{CM}}$	$\zeta_{\text{ML}}$	$\zeta_{\text{CM}}$	
1.25–109	$3.6 \pm 0.2$	<b><math>4.1 \pm 0.3</math></b>	$4.3 \pm 0.3$	<b><math>4.6 \pm 0.4</math></b>	Smallest LISST bin
2.42–109	$4.0 \pm 0.2$	<b><math>4.3 \pm 0.4</math></b>	$4.7 \pm 0.3$	$4.8 \pm 0.4$	Kostadinov et al. [2012]
3.38–109	$4.4 \pm 0.2$	<b><math>4.6 \pm 0.4</math></b>	$4.9 \pm 0.4$	$5.0 \pm 0.5$	Reynolds et al. [2010]
5.55–109	$5.0 \pm 0.3$	$5.1 \pm 0.4$	$5.0 \pm 0.4$	$5.1 \pm 0.6$	Buonassissi and Dierssen [2010]

<sup>a</sup>Comparison of the exponent of the power law parameterization using different size ranges and two curve fitting algorithms. Values are averages  $\pm$  standard deviations within the mixed layer,  $\zeta_{\text{ML}}$ , and at  $Z_{\text{CM}}$ ,  $\zeta_{\text{CM}}$ . Values in bold indicate significant difference (two-tailed  $t$  test, for  $p < 0.05$ ) between the exponent at  $Z_{\text{CM}}$  and the exponent within the mixed layer.

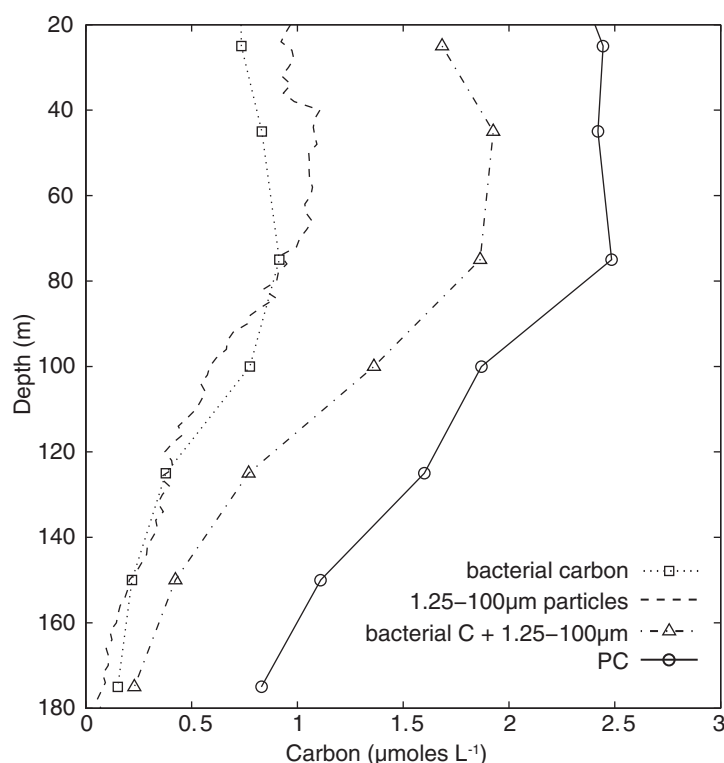


**Figure 7.** Comparison of the carbon concentration in particles and cells measured by different methodologies. Bacterial carbon refers to the sum of the carbon biomass of chlorophyll *a* containing and nonpigmented picoplankton, as determined by flow cytometry (average coefficient of variation = 0.15). Also depicted are estimates of carbon associated with LISST-derived particle measurements in the 1.25–100  $\mu\text{m}$  size range (average coefficient of variation = 0.27). The sum of bacterial carbon and LISST-derived particle biomass (Bacterial C + 1.25–100  $\mu\text{m}$ ) are depicted for those discrete depths where flow cytometric cell abundance measurements were conducted (average coefficient of variation = 0.17). PC depicts particulate carbon concentrations measured with traditional filtration/combustion methodologies (average coefficient of variation = 0.16).

compute particle abundances. This approach provided vertical sampling resolution (2 m) at scales significantly finer than possible using traditional particle sampling methodologies. These observations were used to understand the contribution of different particle sizes to bulk particulate material in this ecosystem, and to assess the effect of physical and ecological processes on the PSD.

#### 4.1. Considerations for Use of Laser Diffraction in an Oligotrophic Setting

We outlined a set of guidelines for the deployment and interpretation of LISST data in oligotrophic oceanic environments that builds on the work by other authors who have previously identified some of the limitations of laser diffraction in oligotrophic settings [e.g., Andrews *et al.*, 2011]. In particular, deployments should be conducted in a manner that minimizes contamination by ambient light; we achieved this by conducting nighttime casts. The influence of bubbles in the surface mixed layer should also be considered; we excluded the upper 20 m in order to negate this potential source of error that was detected as an increase in particle volume, especially for particles with diameters  $>20 \mu\text{m}$ . Future assessments should take into account the bubble penetration depth for the site of study. Scattering by density gradients affects the inner rings of the LISST [Styles, 2006]; we suspect the persistent maximum of particles  $>109 \mu\text{m}$  observed at  $Z_{M5}$  may reflect scattering due to changes in seawater density as the volumetric concentration of these particles correlated with the Brunt-Väisälä frequency (data not shown). Hence, we excluded bins  $>109 \mu\text{m}$  from our analyses. Furthermore, we note that the scattering signal in deep water ( $\sim 200 \text{ m}$ ) approximates a clean water signal. We recommend use of deep clear water signal as a blank in order to account for any influence of the deployment procedures on the instrument function, under the assumption that the optical properties of the depth horizon considered do not change during the course of the study. Lastly, particles smaller than the instrument detection limit (1.25  $\mu\text{m}$ ) can affect the LISST estimates of particle concentrations [Traykovski *et al.*,

mixed-layer of this oligotrophic habitat was influenced by temporal changes in phytoplankton size and community composition.

#### 4. Discussion

We sought to utilize measurements of forward angle light scatter to characterize the temporal and vertical variability in the particle size distribution and particle volume of an important size fraction (1.25–100  $\mu\text{m}$ ) of particulate material in the persistently oligotrophic waters of the NPSG. Although particle scattering is lower in oligotrophic environments than in coastal and eutrophic settings, our measurements were consistently and significantly higher than the signal attributable to particle-free water in the selected ranges of particle size (1.25–100  $\mu\text{m}$ ) and depth (20–180 m, Figure 1a). By using an in situ bio-optical approach, we obtained high-resolution information on particle volume and size, and we used this information to com-

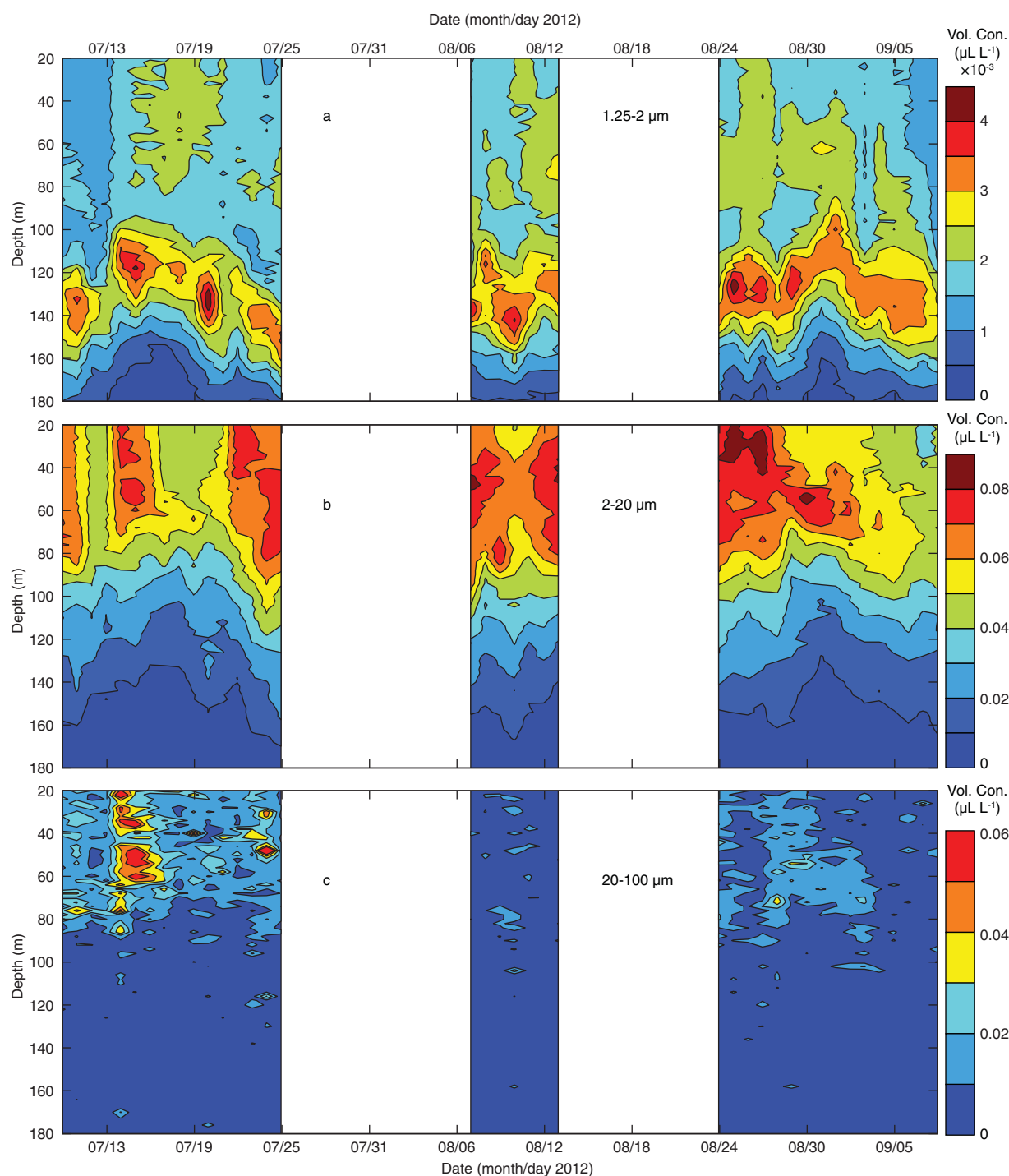


**Figure 8.** Temporal variability associated with particle volumetric concentration in three size fractions: (a) 1.25–2  $\mu\text{m}$ , (b) 2–20  $\mu\text{m}$ , and (c) 20–100  $\mu\text{m}$ .

1999; Andrews *et al.*, 2011], resulting in an overestimation of volumetric concentrations particularly in the smallest size class adopted in this study (1.25–2  $\mu\text{m}$  particles). Submicron particles likely do not contribute significantly to forward scatter, so we suspect the LISST measurements are mostly affected by particles  $\sim 1$   $\mu\text{m}$ , which could include small picoeukaryotes and large bacterial cells. We further discuss the implication of this effect in a later section. After these considerations, we find that TPV tracks beam attenuation and PC and

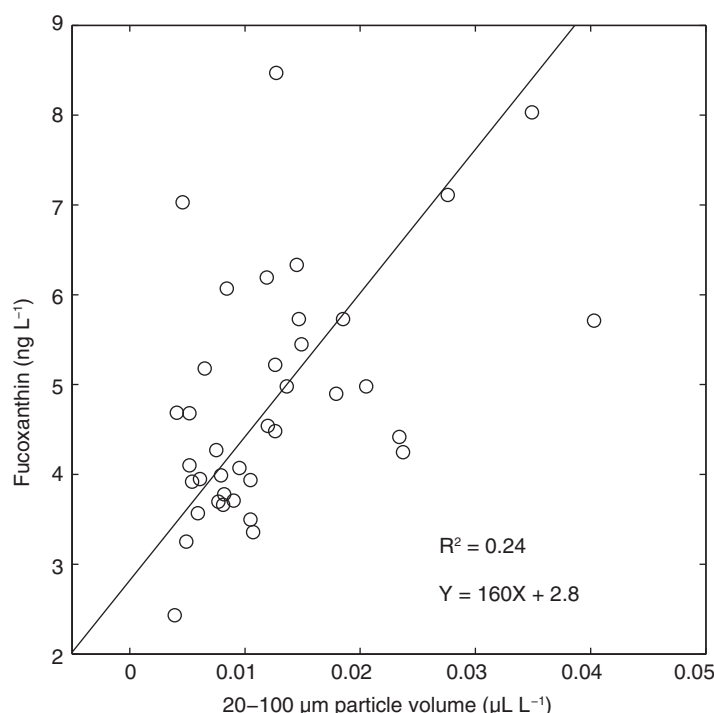


**Figure 9.** Relationships between concentrations of the diatom biomarker fucoxanthin at 25 m and average mixed layer 20–100  $\mu\text{m}$  particle volume. Circles represent observations while lines are results of Model II least squares linear regression analyses (geometric mean regression).

presents the following problems: (1) the PSDs in this setting and others [Jonasz, 1983; Reynolds *et al.*, 2010] show divergence from a simple power law; (2) there is a need to somewhat arbitrarily exclude outer and inner rings which are sensitive to instrument artifacts and deviations from a power law distribution; and (3) the common means for fitting these spectra are biased. In this study, we observed important deviations from a power law distribution that were particularly evident within the mixed layer, where the steepness of the PSD increased for particles  $>6\ \mu\text{m}$  (Figure 5a). A similar change in steepness was previously reported from the open Baltic Sea by Jonasz [1983], who modeled the PSD through two power law functions, with the steeper region starting at  $\sim 6\ \mu\text{m}$ , and characterized by an exponent of  $5.0 \pm 0.6$  (indistinguishable from the exponent computed in this study for particles  $>5.55\ \mu\text{m}$ , Table 2). As a consequence of the deviations from a single power law, the choice of the size range for the fitting critically affected estimates of model parameters (Table 2). Unfortunately, different studies have used different size limits to compute the power law parameterization (examples in Table 2). Furthermore, all published values we could find have used a linearized model to fit a power law to PSD measured with laser diffraction [Reynolds *et al.*, 2010; Buonassissi and Dierssen, 2010; Kostadinov *et al.*, 2012; Xi *et al.*, 2014], but this model presents some biases [see Clauset *et al.*, 2009]; such choice affects the computation of  $\xi$ , when compared to an alternative fitting procedure (Table 2). As an exercise, we have nonetheless compared PSD fits from Station ALOHA to the study by Buonassissi and Dierssen [2010] considering that their exclusion of particles  $<5.55\ \mu\text{m}$  minimized the dependence on the fitting algorithm in our data set. Buonassissi and Dierssen [2010] reported a mean  $\xi$  value of 3.6 (ranging from 2.7 to 4.7) for surface waters of different environments including open ocean sites and river plumes. In comparison, our nonlinear fits for the 5.55–102.95  $\mu\text{m}$  size range gave values of  $\xi$  between 4.41 and 5.78, averaging 4.98 (whereas linearized fits resulted in  $\xi$  between 4.23 and 5.85). These elevated values of  $\xi$  derived for Station ALOHA are presumably characteristic of low-nutrient subtropical gyres, and hence reflect the small size of phytoplankton in oligotrophic environments [Chisholm, 1992]. However, the absolute value is highly dependent on the method of fitting as well as the size range considered; thus, we recommend that the exponent of the PSD not be applied to LISST data until a standard protocol is determined.

#### 4.2. Influences of Phytoplankton Abundance and Size on the Particle Size Distribution

One of the aims of this study was to determine whether specific size classes tracked changes in the phytoplankton community. We found evidence that specific LISST size ranges correspond to the abundance of

that distinct size classes track the vertical or temporal variability of other proxies for distinct phytoplankton groups.

Beam attenuation in the red region of the visible spectrum depends mostly on particle scattering hence on the concentration of particles suspended in the seawater, particularly those in the  $\sim 0.5\text{--}10\ \mu\text{m}$  size range [Stramski and Kiefer, 1991]. While previous studies have demonstrated strong correlations between beam attenuation and PC [e.g., Bishop, 1999], we found that TPV was also correlated with beam attenuation, despite the different size-sensitivities of these two optical proxies for particle load.

Finally, our results indicate that describing relative particle size with the exponent of a power law for purposes of comparison to other environments

eukaryotic phytoplankton and the concentration of pigment markers for diatoms in this region. Both the abundance of small particles (1.25–2  $\mu\text{m}$ ) and the concentration of photosynthetic eukaryotes peak at the depth of the chlorophyll *a* maximum (Figures 3d and 4). From this observation, we conclude that (1) eukaryotic cells counted via flow cytometry are dominated by picoeukaryotes (with a diameter  $<2 \mu\text{m}$ ), not surprisingly given the sharp decrease of phytoplankton abundance with cell size [Stramski and Kiefer, 1991]; and (2) that detritus and heterotrophic organisms represent a small fraction of the 1.25–2  $\mu\text{m}$  particles. Picoeukaryotes ( $<2 \mu\text{m}$ ) are known to be associated with the DCM and higher nitrate concentrations in this region [Worden and Not, 2008]. These organisms are difficult to identify unambiguously via microscopy since they do not have distinctive morphological features; flow cytometry, HPLC-based pigments, and picoeukaryote gene surveys currently provide the best information on the vertical or temporal distributions of these organisms. These methods all provide valuable yet coarse information on the abundance of a key group of organisms. While future work needs to be conducted to verify that the LISST retrievals of small particles (1.25–2  $\mu\text{m}$ ) does in fact correspond to the abundance of picoeukaryotes, we believe this approach shows great promise for measurement of the temporal and spatial variability of picoeukaryotes in oligotrophic regimes. For instance, if we assume that the abundance of this size class at the DCM represents picoeukaryote populations, we find that cell abundances vary by a factor of  $\sim 2$  over daily to weekly time scales. This variability may reflect the balance of growth and loss processes specific to picoeukaryotes. Further work, perhaps combining flow sorting and laser diffraction, can address these hypotheses.

The second major finding of this study was that fucoxanthin concentrations correlated well with the concentration of 20–100  $\mu\text{m}$  particles (Figure 9). Furthermore, we measured rapid (daily scale) changes in concentrations of both fucoxanthin and 20–100  $\mu\text{m}$  particles including a pronounced accumulation of 20–100  $\mu\text{m}$  particles just below the mixed layer that dissipated rapidly on subsequent days. Taken together, these results suggest diatom population dynamics in the oligotrophic North Pacific are highly variable both in time and depth; hence, elucidating the influence of these organisms on biogeochemistry and ecology of this system will demand highly resolved (in space and time) sampling strategies.

#### 4.3. Contribution of Different Size Fractions to Particulate Material

The above results indicate the biological relevance of LISST retrievals of two specific particle size classes (1.25–2.0 and 20–100  $\mu\text{m}$ ). Although 1.25–2  $\mu\text{m}$  particles were the most abundant particles at depths  $>100 \text{ m}$ , among the size range considered here (1.25–100  $\mu\text{m}$ ), particles in the 3–10  $\mu\text{m}$  fraction were the most important contributors to particle volume throughout the euphotic zone. Our observations on the importance of these particles appear consistent with previous reports using the LISST-100X in other marine ecosystems, including more eutrophic habitats. In the Santa Barbara Channel, Kostadinov *et al.* [2012] observed that particles  $\sim 6 \mu\text{m}$  in diameter dominated the volumetric concentration. Similarly, a study conducted in nearshore waters of the California Current found particles 4–5  $\mu\text{m}$  in diameter were major contributors to the particle volumetric concentration [Reynolds *et al.*, 2010]. The similarity between our observations and measurements conducted as part of these other studies is somewhat surprising considering that these other sites were characterized by particle volumetric concentrations approximately an order of magnitude greater than observed at Station ALOHA. Nonetheless, our observations suggest that even in the persistently oligotrophic waters of the NPSG, particles in the 3–10  $\mu\text{m}$  size range are significant contributors to particulate matter stocks. Although our observations highlight the importance of the 3–10  $\mu\text{m}$  particles, at present we are unable to determine the composition, trophic role, or turnover rates of these particles, limiting our understanding of their role in upper ocean biogeochemistry, including their contribution to the vertical export of organic matter.

We also estimated carbon concentrations associated with 1.25–100  $\mu\text{m}$  particles. Based on carbon:cell biovolume conversions, our results suggest that these particles accounted for  $\sim 40\%$  (ranging 30–53%) of the measured PC in the upper euphotic zone (25–75 m). This estimate was similar to the derived carbon contribution attributable to phototrophic bacteria and nonpigmented picoplankton (presumably mostly organisms  $<1 \mu\text{m}$  in diameter), which together averaged 35% (ranging from 25 to 48%) of the measured PC in the same depth range. The remaining  $\sim 25\%$  of measured PC in the upper water column can be explained by: (1) particles greater than 100  $\mu\text{m}$ ; (2) detritus and eukaryotes  $<1.25 \mu\text{m}$ ; and to a lesser extent (3) the retention of dissolved organic carbon on glass fiber filters which would cause an overestimation of PC concentrations [Karl *et al.*, 1998]. Notably, the residual amount of carbon from the subtraction of the contribution by bacteria and 1.25–100  $\mu\text{m}$  particles to PC was very similar to the concentration of PC at 200 m ( $\sim 0.7 \mu\text{mol L}^{-1}$ ), where no particles could be detected using laser diffraction. If we assume that this “background” PC is uniformly

distributed in the upper 200 m, then the complete PC inventory can be accounted for; further characterization of the nature and size distribution of this deep material is necessary to validate this assumption.

The major assumption underlying the comparison of carbon stocks is that the carbon contained in bacteria and archaea, and the carbon contained in particles 1.25–100  $\mu\text{m}$  in diameter, represent separate stocks. One complication in this approach derives from the sensitivity of the LISST to the presence of particles below the manufacturer declared lower size limit, 1.25  $\mu\text{m}$  [Andrews et al., 2011]. The sensitivity of the instrument to these out-of-range particles decreases for particles smaller than 1  $\mu\text{m}$  because of their reduced scattering in the forward direction [Andrews et al., 2011]. Considering this size dependence, we believe that our assumption of separated bacterial and LISST-derived carbon stocks is a reasonable approximation in the case of Station ALOHA due to the small size of the dominant bacterial populations: *Prochlorococcus* [Chisholm et al., 1988; Morel et al., 1993], and the SAR11 clade [Rappé et al., 2002]. The largest bacterial cells might influence LISST measurements, but such cells are generally not very abundant. One exception is *Synechococcus* which has diameters  $\sim 1 \mu\text{m}$ , but that represented a maximum of 4% of the total bacterial carbon in our study. It must also be stressed that the transformation of particle volume to cell counts and of cell counts to carbon biomass estimates derive from static parameterizations that cannot account for inherent physiological variability of living cells. For example, the cellular carbon quota of *Prochlorococcus* greatly varies with depth and in time [Casey et al., 2013], while various approaches report carbon quotas for heterotrophic bacteria at Station ALOHA between 6 and 20 fg C cell<sup>-1</sup> [Kawasaki et al., 2011; Campbell et al., 1994; Christian and Karl, 1994]. Similarly, the volume to carbon conversion used for 1.25–100  $\mu\text{m}$  particles overestimates carbon concentration in the presence of high abundances of diatoms [Menden-Deuer and Lessard, 2000], or aggregates, that in cultures have been shown to have lower mass density than plankton [Verity et al., 2000]. Finally, natural particle populations include important departures from the spherical shape assumed in the reconstruction of PSD from laser diffraction, so that both particle shape and particle orientation affect measurements of forward scattering [Karp-Boss et al., 2007]. While the effect of this divergence on the shape of size spectra is still difficult to quantify, to a first degree we can assume that it causes an overestimation of both particle volume and particle carbon. This assumption relies on the considerations that forward angle scattering is proportional to the cross-sectional area of a particle and that a sphere is the shape with the greatest volume: cross-sectional area ratio for randomly oriented particles [Karp-Boss et al., 2007].

#### 4.4. Physical Influences on the Particle Size Distribution

The high vertical and temporal resolution bio-optical measurements conducted as part of this study provided insight into the role of physical processes in shaping particle distributions at Station ALOHA. In particular, the vertical extent of upper ocean mixing appeared to affect the vertical distribution of particles during our study. We observed consistent maxima of both 2–20  $\mu\text{m}$  particles and TPV near the base of the surface mixed layer (Figures 3b and 3e and Table 1). The accumulation of particles below the mixed layer can be interpreted in several ways, including settling of particulate matter out of the mixed layer due to turbulence enhanced export [Ruiz et al., 2004]. However, this explanation seems unlikely because decreased residence time of particles in the mixed layer would be effective only if turbulence was vertically homogeneous, an assumption that seems unlikely for a mixed layer generated by interactions at the sea surface [Ross, 2006]. An alternative explanation for particle accumulation is that the base of the mixed layer may represent a favorable environment for the growth of certain planktonic species. Organisms growing in the mixed layer may be intermittently exposed to highlight intensities (including ultraviolet radiation) that could result in damage to DNA [Jeffrey et al., 1996] and negatively affect the functionality of the photosystems of phytoplankton cells [Villafañe et al., 1998]. Such a mechanism would imply decoupling in growth and removal at the base of the mixed layer relative to the mixed layer. Unfortunately, our measurements do not allow us to determine whether particle maxima represent an increase in phytoplankton biomass at the base of the mixed layer. Vertical profiles of chlorophyll from calibrated fluorescence do not show maxima at the base of the mixed layer, but photoacclimation [Geider et al., 1998] generates a strong vertical gradient in the phytoplankton chlorophyll *a* to carbon ratio that makes it difficult to reconstruct the vertical variation of phytoplankton biomass from pigment concentrations.

#### 5. Conclusions

Our results highlight the strong vertical and temporal dynamics in the size distribution of particle abundance and volume for the 1.25–109  $\mu\text{m}$  size range in the euphotic zone of the North Pacific Subtropical

Gyre. These observations may be seen as a piece of the puzzle in our effort to understand the effects that physical and biological processes have on the production, accumulation, and consumption of particulate organic matter. While there are limitations to our approach, we have outlined specific recommendations for the deployment and analysis of LISST data in an oligotrophic setting. If measurements of the PSD at these high temporal and spatial scales could be combined and/or validated with analyses that allowed for visualization and verification of the nature and taxonomy of particles across the microbial size spectrum, a number of outstanding issues in marine microbial ecology could be resolved. For example, one could explore niche differentiation at unprecedented scales, or evaluate hypotheses about the relationship between the rate of community production and phytoplankton size.

## Acknowledgments

The data for this paper are available on the ftp server of the School of Ocean and Earth Science and Technology of the University of Hawaii (<ftp://ftp.soest.hawaii.edu/dkarl/cmored/publication-data>); please contact the authors to obtain raw LISST data files. We thank the captain and crew of the R/V Kilo Moana and the Ocean Technology Group of the University of Hawaii for their assistance at sea. We acknowledge Sam Wilson (University of Hawaii) for the useful discussions on the ecological and biogeochemical processes observed during HOE-DYLAN. We also thank Eric Grabowski and Ken Doggett (University of Hawaii) for analyses of particulate carbon and cell counts using flow cytometry, respectively. Discussions with Amanda Briggs-Whitmire (Oregon State University) on laser diffraction greatly improved our understanding of data post-processing. We are grateful to Emmanuel Boss and one anonymous reviewer who provided helpful comments on this manuscript. This research was supported by the National Science Foundation through grants to the Center for Microbial Oceanography: Research and Education (C-MORE; EF0424599 to D.M.K.) and the Hawaii Ocean Time-series (OCE-0926766 and OCE-1260164 to M.J.C., D.M.K., and R.R.B.), by the Gordon and Betty Moore Foundation (to D.M.K.), and by the National Aeronautics and Space Administration New Investigator Program (NNX10AQ81G to A.E.W.).

## References

- Agrawal, Y. C., and H. C. Pottsmith (2000), Instruments for particle size and settling velocity observations in sediment transport, *Mar. Geol.*, **168**, 89–114, doi:10.1016/S0025-3227(00)00044-X.
- Andrews, S. W., D. M. Nover, J. E. Reuter, and S. G. Schladow (2011), Limitations of laser diffraction for measuring fine particles in oligotrophic systems: Pitfalls and potential solutions, *Water Resour. Res.*, **47**, W05523, doi:10.1029/2010WR009837.
- Bader, H. (1970), The hyperbolic distribution of particle sizes, *J. Geophys. Res.*, **75**, 2822–2830, doi:10.1029/JC075i015p02822.
- Bidigare, R. R., L. Van Heukelem, and C. C. Trees (2005), Analysis of algal pigments by high-performance liquid chromatography, in *Algal Culturing Techniques*, edited by R. A. Andersen, pp. 327–345, Academic, Burlington, Mass.
- Bishop, J. K. B. (1999), Transmissometer measurement of POC, *Deep Sea Res., Part I*, **46**, 353–369, doi:10.1016/S0967-0637(98)00069-7.
- Bishop, J. K. B., and T. J. Wood (2008), Particulate matter chemistry and dynamics in the twilight zone at VERTIGO ALOHA and K2 sites, *Deep Sea Res., Part I*, **55**, 1684–1706, doi:10.1016/j.dsr.2008.07.012.
- Boss, E. S., M. Twardowski, and S. Herring (2001), Shape of the particulate beam attenuation spectrum and its inversion to obtain the shape of the particulate size distribution, *Appl. Opt.*, **40**, 4885–4893, doi:10.1364/AO.40.004885.
- Brown, J. H., J. F. Gillooly, A. P. Allen, and V. M. Savage (2004), Toward a metabolic theory of ecology, *Ecology*, **85**, 1771–1789.
- Buitenhuis, E. T., et al. (2012), Picophytoplankton biomass distribution in the global ocean, *Earth Syst. Sci. Data*, **4**, 37–46, doi:10.5194/essd-4-37-2012.
- Buonassissi, C. J., and H. M. Dierssen (2010), A regional comparison of particle size distributions and the power law approximation in oceanic and estuarine surface waters, *J. Geophys. Res.*, **115**, C10028, doi:10.1029/2010JC006256.
- Burd, A. B., and G. A. Jackson (2009), Particle aggregation, *Ann. Rev. Mar. Sci.*, **1**, 65–90, doi:10.1146/annurev.marine.010908.163904.
- Campbell, L., H. Nolla, and D. Vulot (1994), The importance of *Prochlorococcus* to community structure in the Central North Pacific Ocean, *Limnol. Oceanogr.*, **39**, 954–961.
- Casey, J. R., J. P. Aucan, S. R. Goldberg, and M. W. Lomas (2013), Changes in partitioning of carbon amongst photosynthetic pico- and nano-plankton groups in the Sargasso Sea in response to changes in the North Atlantic Oscillation, *Deep Sea Res., Part II*, **93**, 58–70, doi:10.1016/j.dsr.2.2013.02.002.
- Chisholm, S. W. (1992), Phytoplankton size, in *Primary Productivity and Biogeochemical Cycles in the Sea*, edited by P. G. Falkowski and A. D. Woodhead, pp. 213–237, Plenum, N. Y.
- Chisholm, S. W., R. J. Olson, E. R. Zettler, R. Goericke, J. B. Waterbury, and N. A. Welschmeyer (1988), A novel free-living prochlorophyte abundant in the oceanic euphotic zone, *Nature*, **334**, 340–343, doi:10.1038/334340a0.
- Christian, J. R., and D. M. Karl (1994), Microbial community structure at the U.S.-Joint Global Ocean Flux Study Station ALOHA: Inverse methods for estimating biochemical indicator ratios, *J. Geophys. Res.*, **99**, 14269–14276, doi:10.1029/94JC00681.
- Clauset, A., C. R. Shalizi, and M. E. J. Newman (2009), Power-law distributions in empirical data, *SIAM Rev.*, **51**, 661–703, doi:10.1137/070710111.
- de Boyer Montégut, C., G. Madec, A. S. Fischer, A. Lazar, and D. Iudicone (2004), Mixed layer depth over the global ocean: An examination of profile data and a profile-based climatology, *J. Geophys. Res.*, **109**, C12003, doi:10.1029/2004JC002378.
- Geider, R. J., H. L. MacIntyre, and T. M. Kana (1998), A dynamic regulatory model of phytoplanktonic acclimation to light, nutrients, and temperature, *Limnol. Oceanogr.*, **43**, 679–694, doi:10.4319/lo.1998.43.4.0679.
- Hebel, D. V., and D. M. Karl (2001), Seasonal, interannual and decadal variations in particulate matter concentrations and composition in the subtropical North Pacific Ocean, *Deep Sea Res., Part II*, **48**, 1669–1695, doi:10.1016/S0967-0645(00)00155-7.
- Jeffrey, W. H., R. J. Pledger, P. Aas, S. Hager, R. B. Coffin, R. Von Haven, and D. L. Mitchell (1996), Diel and depth profiles of DNA photodamage in bacterioplankton exposed to ambient solar ultraviolet radiation, *Mar. Ecol. Prog. Ser.*, **137**, 283–291, doi:10.3354/meps137283.
- Jonasz, M. (1983), Particle-size distributions in the Baltic, *Tellus, Ser. B*, **35**, 346–358, doi:10.3402/tellus.v35i5.14624.
- Jones, D., and M. S. Wills (1956), The attenuation of light in sea and estuarine waters in relation to the concentration of suspended solid matter, *J. Mar. Biol. Assoc. U. K.*, **35**, 431–444, doi:10.1017/S0025315400010250.
- Karl, D. M., D. V. Hebel, K. Björkman, and R. M. Letelier (1998), The role of dissolved organic matter release in the productivity of the oligotrophic North Pacific Ocean, *Limnol. Oceanogr.*, **43**, 1270–1286, doi:10.4319/lo.1998.43.6.1270.
- Karp-Boss, L., L. Azevedo, and E. S. Boss (2007), LISST-100 measurements of phytoplankton size distribution: Evaluation of the effects of cell shape, *Limnol. Oceanogr. Methods*, **5**, 396–406, doi:10.4319/lom.2007.5.396.
- Kawasaki, N., R. Sohrin, H. Ogawa, T. Nagata, and R. Benner (2011), Bacterial carbon content and the living and detrital bacterial contributions to suspended particulate organic carbon in the North Pacific Ocean, *Aquat. Microb. Ecol.*, **62**, 165–176, doi:10.3354/ame01462.
- Kindler, K., A. Khalili, and R. Stocker (2010), Diffusion-limited retention of porous particles at density interfaces, *Proc. Natl. Acad. Sci. U. S. A.*, **107**, 22,163–22,168, doi:10.1073/pnas.1012319108.
- Kostadinov, T. S., D. A. Siegel, S. Maritorena, and N. Guillocheau (2012), Optical assessment of particle size and composition in the Santa Barbara Channel, California, *Appl. Opt.*, **51**, 3171–3189, doi:10.1364/AO.51.003171.
- Laws, E. A., R. M. Letelier, and D. M. Karl (2014), Estimating the compensation irradiance in the ocean: The importance of accounting for non-photosynthetic uptake of inorganic carbon, *Deep Sea Res., Res. I*, **93**, 35–40, doi:10.1016/j.dsr.2014.07.011.
- Lorenzen, C. J. (1966), A method for the continuous measurement of in vivo chlorophyll concentration, *Deep Sea Res. Oceanogr. Abstr.*, **13**, 223–227, doi:10.1016/0011-7471(66)91102-8.
- MacIntyre, S., A. L. Alldredge, and C. C. Gotschalk (1995), Accumulation of marine snow at density discontinuities in the water column, *Limnol. Oceanogr.*, **40**, 449–468.

- Menden-Deuer, S., and E. J. Lessard (2000), Carbon to volume relationships for dinoflagellates, diatoms, and other protist plankton, *Limnol. Oceanogr.*, **45**, 569–579, doi:10.4319/lo.2000.45.3.0569.
- Merrifield, M. A., P. E. Holloway, and T. M. S. Johnston (2001), The generation of internal tides at the Hawaiian Ridge, *Geophys. Res. Lett.*, **28**, 559–562, doi:10.1029/2000GL011749.
- Mikkelsen, O. A., T. G. Milligan, P. S. Hill, R. J. Chant, C. F. Jago, S. E. Jones, V. Krivtson, and G. Mitchelson-Jacob (2008), The influence of schlieren on in situ optical measurements used for particle characterization, *Limnol. Oceanogr. Methods*, **6**, 133–143, doi:10.4319/lom.2008.6.133.
- Morel, A., Y.-H. Ahn, F. Partensky, D. Vaulot, and H. Claustre (1993), *Prochlorococcus* and *Synechococcus*: A comparative study of their optical properties in relation to their size and pigmentation, *J. Mar. Res.*, **51**, 617–649, doi:10.1357/0022240933223963.
- Rappé, M. S., S. A. Connon, K. L. Vergin, and S. J. Giovannoni (2002), Cultivation of the ubiquitous SAR11 marine bacterioplankton clade, *Nature*, **418**, 630–633, doi:10.1038/nature00917.
- Reynolds, R. A., D. Stramski, V. M. Wright, and S. B. Woźniak (2010), Measurements and characterization of particle size distributions in coastal waters, *J. Geophys. Res.*, **115**, C08024, doi:10.1029/2009JC005930.
- Rienecker, E., J. Ryan, M. Blum, C. Dietz, L. Coletti, R. Marin III, and W. P. Bissett (2008), Mapping phytoplankton in situ using a laser-scattering sensor, *Limnol. Oceanogr. Methods*, **6**, 153–161.
- Ross, O. N. (2006), Particles in motion: How turbulence affects plankton sedimentation from an oceanic mixed layer, *Geophys. Res. Lett.*, **33**, L10609, doi:10.1029/2006GL026352.
- Ruiz, J., D. Macías, and F. Peters (2004), Turbulence increases the average settling velocity of phytoplankton cells, *Proc. Natl. Acad. Sci. U. S. A.*, **101**, 17,720–17,724, doi:10.1073/pnas.0401539101.
- Sieburth, J. M., V. Smetacek, and J. Lenz (1978), Pelagic ecosystem structure: Heterotrophic compartments of the plankton and their relationship to plankton size fractions, *Limnol. Oceanogr.*, **23**, 1256–1263.
- Smayda, T. J. (1970), The suspension and sinking of phytoplankton in the sea, *Oceanogr. Mar. Biol.*, **8**, 353–414.
- Stramski, D., and D. A. Kiefer (1991), Light scattering by microorganisms in the open ocean, *Prog. Oceanogr.*, **28**, 343–383, doi:10.1016/0079-6611(91)90032-H.
- Stramski, D., and J. Tegowski (2001), Effects of intermittent entrainment of air bubbles by breaking wind waves on ocean reflectance and underwater light field, *J. Geophys. Res.*, **106**, 31,345–31,360, doi:10.1029/2000JC000461.
- Styles, R. (2006), Laboratory evaluation of the LISST in a stratified fluid, *Mar. Geol.*, **227**, 151–162, doi:10.1016/j.margeo.2005.11.011.
- Traykovski, P., R. J. Latter, and J. D. Irish (1999), A laboratory evaluation of the laser in situ scattering and transmissometry instrument using natural sediments, *Mar. Geol.*, **159**, 355–367, doi:10.1016/S0025-3227(98)00196-0.
- Vagle, S., C. McNeil, and N. Steiner (2010), Upper ocean bubble measurements from the NE Pacific and estimates of their role in air-sea gas transfer of the weakly soluble gases nitrogen and oxygen, *J. Geophys. Res.*, **115**, C12054, doi:10.1029/2009JC005990.
- Verity, P. G., S. C. Williams, and Y. Hong (2000), Formation, degradation, and mass:volume ratios of detritus derived from decaying phytoplankton, *Mar. Ecol. Prog. Ser.*, **207**, 53–68, doi:10.3354/meps207053.
- Villafañe, V. E., K. Sundbäck, F. L. Figueroa, and E. W. Helbling (1998), Photosynthesis in the aquatic environment as affected by UVR, in *UV Effects in Aquatic Organisms and Ecosystems*, edited by E. W. Helbling and H. E. Zagarese, pp. 357–397, The R. Soc. of Chem., Cambridge, U. K.
- Worden, A. Z., and F. Not (2008), Ecology and diversity of picoeukaryotes, in *Microbial Ecology of the Oceans*, 2nd ed., edited by D. L. Kirchman, pp. 159–205, John Wiley, Hoboken, N. J.
- Xi, H., P. Larouche, S. Tang, and C. Michel (2014), Characterization and variability of particle size distributions in Hudson Bay, Canada, *J. Geophys. Res. Ocean*, **119**, 3392–3406, doi:10.1002/2013JC009542.